Vegetable Research

ARTICLE

Open Access

https://doi.org/10.48130/vegres-0025-0026

Vegetable Research **2025**, 5: e032

Physiological and transcriptomic insights into selenite-induced stress responses in *Cucurbita moschata* seedlings

Yong Wang[1,2], Longyu Wang[1,2], Naveed Mushtaq[3], Weina Liu[4], Tao Zhang[1], Yanman Li[1], Jingwen Wang[1], Luming Yang[1,2], Shouru Sun[1,2*] and Lei Zhu[1,2*]

[1] *College of Horticulture, Henan Agricultural University, Zhengzhou 450002, China*
[2] *Henan Engineering Technology Research Center of Germplasm Innovation and Utilization of Melon Crops, Henan Agricultural University, Zhengzhou 450002, China*
[3] *Key Laboratory for Quality Regulation of Tropical Horticultural Crops of Hainan Province, School of Tropical Agriculture and Forestry, Hainan University, Danzhou 571737, China*
[4] *Henan Zhongwei Chunyu Plant Nutrition Co., Ltd., Zhengzhou 450000, China*
* Corresponding authors, E-mail: ssr365@henau.edu.cn; zhulei2018@henau.edu.cn

Abstract

Selenium (Se)-enriched plants constitute important dietary sources of Se for human nutrition, and selenite is one of the dominant forms of Se available to plants in soil. However, the threshold between beneficial and phytotoxic selenite levels in soil remains narrow, posing challenges for plant growth. This study investigated the effects of selenite concentrations (2–80 μM) on growth parameters and Se accumulation in *Cucurbita moschata* seedlings. The findings showed significant stress effects under all except 2 μM selenite treatments, and demonstrated a dose-dependent toxic effect and Se accumulation in both shoots and roots. Concentrations exceeding 40 μM not only induced elevated superoxide radical ($O_2^{\cdot-}$) accumulation but also caused significant growth inhibition and visible toxicity symptoms, and these adverse effects were significantly mitigated by exogenous melatonin application, so 40 μM selenite treatment was selected for RNA-seq. Transcriptomic analysis revealed the activation of a suite of defense mechanisms in roots under selenite stress, encompassing Ca^{2+} signaling, ethylene and jasmonate signaling, antioxidant defense systems, the MAPK cascade, and melatonin synthesis. Furthermore, the study identified candidate genes potentially involved in Se uptake and metabolism, including genes encoding phosphate and sulfate transporters, adenosine triphosphate sulfurylase, adenosine phosphosulfate kinase, adenosine phosphosulfate reductase, sulfite reductase, glutathione reductase, and cysteine synthases. These findings enhance understanding of the physiological and molecular mechanisms underlying Se accumulation and tolerance to Se toxicity in *C. moschata* and provide genetic targets and a theoretical foundation for breeding Se-enriched pumpkin varieties with enhanced stress resilience.

Citation: Wang Y, Wang L, Mushtaq N, Liu W, Zhang T, et al. 2025. Physiological and transcriptomic insights into selenite-induced stress responses in *Cucurbita moschata* seedlings. *Vegetable Research* 5: e032 https://doi.org/10.48130/vegres-0025-0026

Introduction

Pumpkin (*Cucurbita moschata* Duch.) is a species belonging to the Cucurbitaceae family. Pumpkins and pumpkin byproducts (seeds, leaf, and skin/peel) are widely used as functional foods by people because of their various bioactive compounds, including Selenium (Se)[1]. Se is thought of as an indispensable trace element for human health[2], while it has one of the narrowest ranges between dietary deficiency (< 40 μg·d^{-1}) and toxicity (> 400 μg·d^{-1})[3]. Plants are the primary source of dietary Se for humans and animals, as they absorb inorganic Se from the soil and convert it into organic forms[4]. Se concentrations in most global soils are low (ranging from 0.01 to 2.0 mg·kg^{-1}, mean ~0.4 mg·kg^{-1}), except in seleniferous soils associated with specific geological features where concentrations can exceed 10 mg·kg^{-1}[4]. Biofortification is a key strategy to alleviate Se deficiency in low-Se regions, while phytoremediation is employed in seleniferous areas to mitigate Se toxicity[4].

While the essentiality of Se for higher plants remains uncertain, it can enhance plant growth, quality, and tolerance to diverse biotic and abiotic stresses[5,6]. Previous studies have reported that Se can enhance the activities of antioxidant enzymes, such as catalase (CAT), peroxidase (POD), and superoxide dismutase (SOD), thereby mitigating stress-induced reactive oxygen species (ROS) accumulation in plants[7–11]. However, at high concentrations, Se becomes phytotoxic and results in Se stress for plant growth, such as damaging plant cells and inhibiting shoot and root growth[8,12–14]. Se toxicity primarily arises from two mechanisms: the misincorporation of Se-amino acids (e.g., selenocysteine [SeCys], selenomethionine [SeMet]) into proteins, leading to malfunctional proteins, and the induction of oxidative stress[4,5,11]. Grant et al.[15] demonstrated an interconnection between glutathione (GSH) depletion and ROS accumulation during Se stress in *Arabidopsis*. Melatonin (MT), recognized as a scavenger of stress-induced ROS[16], has been shown to alleviate Se stress in grapevines[14].

Selenite (Se[IV]) and Selenate (Se[VI]) are the dominant forms of Se available to plants in soil, and Se(IV) dominates in neutral and acidic soils, whereas Se(VI) prevails in alkaline soils[17]. Owing to the high chemical similarity between Se and sulfur (S), both Se(IV) and Se(VI) are assimilated via the S metabolic pathway[4]. Additionally, Se(IV) uptake is primarily mediated by phosphate transporters (PHTs) and nodulin 26-like intrinsic proteins (NIPs), and it is readily converted to SeCys and other organic forms through the S assimilation pathway[17]. Se(VI) is first reduced to Se(IV) by ATP sulfurylase (APS) and APS reductase (APR) in plants; subsequently, Se(IV) is reduced to selenide (H_2Se^- or Se^{2-}) by sulfite reductase (SiR); Selenide is then incorporated into O-acetylserine (OAS) by cysteine synthase (CS) to form SeCys; SeCys can be further metabolized to other compounds, such as SeMet, by a series of enzymes[17]. The Se assimilation and roles in plants have been briefly summarized and presented in Fig. 1. Lintschinger et al.[18] observed significant interspecific variation in Se absorption rates. Overexpression of genes involved in Se metabolism enhances Se accumulation capacity[19,20]. Thus, it is essential to elucidate the molecular mechanisms of plant

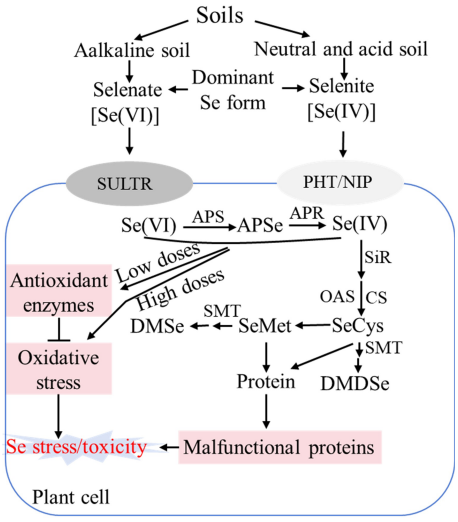

Fig. 1 Schematic diagram showing selenium assimilation pathway and roles in plants. SULTR: Sulfate transporter; PHT: Phosphate transporter; NIP: Nodulin 26-like intrinsic protein. APS: ATP sulfurylase; APSe: Adenosine phosphoselenate; APR: APS reductase; SiR: Sulfite reductase; CS: Cysteine synthase; OAS: O-acetylserine; SeCys: Selenocysteine; SeMet: selenomethionine. SMT: Selenocysteine methyltransferase; DMSe: non-toxic dimethylselenide; DMDSe: dimethyldiselenide; ROS: Reactive oxygen species; Se: Selenium.

Se responses and identify key Se metabolism-related genes, which could facilitate genetic engineering approaches for biofortification and phytoremediation.

Pumpkin is widely cultivated globally, serving not only as a food source but also as a valuable rootstock for other cucurbit crops[21]. However, the molecular mechanisms underlying selenite uptake and metabolism in pumpkin remain poorly understood. In this study, physiological and transcriptomic analyses were performed to investigate selenite-induced responses in *C. moschata*, focusing on selenite toxicity, uptake, and metabolism mechanisms in roots. The findings will improve the understanding of Se accumulation and selenite tolerance in pumpkin. The genetic components identified herein provide a theoretical basis for improving selenite toxicity responses in pumpkin seedlings and inform future breeding and cultivation of Se-enriched pumpkin varieties.

Materials and methods

Plant materials and treatments

The *C. moschata* used in this study, designated WCO39, was provided by the Chinese Vegetable Germplasm Resources Intermediate Bank, and the experiments were carried out in Henan Agricultural University, Zhengzhou, Henan Province, China. Seeds of WCO39 germinated at 28 °C with shaking at 150 rpm on a shaker, were then sown into hole trays within a growth chamber under the following conditions: photosynthetic photon flux density (PPFD) of 200 μmol·m^{-2}·s^{-1}, 16 h light (25 °C)/8 h dark (20 °C) photoperiod. Five days after sowing, uniform seedlings were transferred to 1 L plastic containers filled with half-strength Hoagland's nutrient solution (pH = 6.0) for 3 d. Seedlings were then divided into six groups and irrigated with solutions containing Na_2SeO_3 at concentrations of 0 (Se0), 2 (Se2), 10 (Se10), 20 (Se20), 40 (Se40), or 80 (Se80) μM. Each treatment group consisted of twelve seedlings, with three biological replicates. The nutrient solution was renewed every 3 d. A schematic of the seedling culture and treatment procedure is provided in Supplementary Fig. S1.

Melatonin (MT) treatment experiments followed the previous study[22]. Briefly, seedlings at the first true leaf stage were divided into four groups: (1) Control (Se0): normal nutrient solution + foliar spray of water; (2) MT100: normal nutrient solution + foliar spray of 100 μM MT; (3) Se40: nutrient solution containing 40 μM Na_2SeO_3 + foliar spray of water; (4) Se40MT100: nutrient solution containing 40 μM Na_2SeO_3 + foliar spray of 100 μM MT. Each group consisted of twelve seedlings, with three biological replicates. Foliar application of 100 μM MT (approximately 5 mL per plant) was performed daily at 18:00.

Physiological analysis

Phenotypic analysis for selenite concentration experiments was conducted after 10 d of treatment, and after 13 d for melatonin treatment experiments. Plant height, petiole length, leaf length, and leaf width were measured using a ruler. Hypocotyl diameter was measured using a digital vernier caliper. To determine dry weight (DW), fresh samples were oven-dried at 105 °C for 15 min, followed by drying at 80 °C for 48 h. Both fresh weight (FW) and DW were measured using a microbalance. Chlorophyll was extracted from the second true leaves by homogenization in 80% (v/v) acetone. Absorbance of the extracts was read at 663 and 646 nm using a UV-1800 spectrophotometer[22].

Malondialdehyde (MDA) content and relative electrical conductivity (REC) of the second true leaves were determined as described previously[23]. Superoxide anion ($O_2^{\cdot-}$) accumulation in leaves was visualized via nitro blue tetrazolium (NBT) staining[22], by which $O_2^{\cdot-}$ was shown as a blue dot because of NBT reduction. Briefly, leaves were immersed in a 0.1% NBT solution (pH = 6.4) containing 10 mM sodium azide. The samples were then incubated in darkness at 28 °C until blue spots appeared. For proper visualization, the chlorophyll in leaves was removed with absolute ethanol.

Determination of Se and S contents

To measure the contents of Se and S in the shoots and roots of WCO39 seedlings, the above and below-ground parts were separated and oven-dried at 80 °C for 48 h. The concentrations of total Se and total S were determined according to the Standard Methods GB 5009.93–2010 and GB 5009.268–2016 developed by the Ministry of Health of the People's Republic of China. Accordingly, the dried samples were ground into powder and digested with nitric acid overnight, then put in a constant temperature drying oven maintained at 80 °C for 2 h, followed by 120 °C for 2 h, and finally 160 °C for 4 h. The concentrations were examined using inductively coupled plasma-mass spectrometry (NexION®2000 ICP-MS, PerkinElmer Instrument Co., USA).

For the determination of inorganic Se in shoots and roots, the dried samples were added to hydrogen chloride as described by Li et al.[24]. Samples were placed in a constant temperature water bath at 70 °C, shaken for 2 h, filtered through absorbent cotton, boiled in a water bath for 20 min, and then potassium ferricyanide was added. The concentration of inorganic Se was determined by hydride generation atomic fluorescence spectrometry (HG-AFS, AFS820, Beijing Jitian Instrument Co., China).

As described by Li et al.[24], the concentrations of organic Se in shoots and roots were calculated using the formula: $Se_{organic} = Se_{total} - Se_{inorganic}$, in which $Se_{organic}$, Se_{total}, and $Se_{inorganic}$ represented the organic Se concentration, total Se concentration, and inorganic Se concentration, respectively.

RNA-seq

The roots of WCO39 seedlings were harvested at 24 h under 40 μM selenite treatment (Se40) and normal conditions (Se0) with three biological replicates each treatment. Total RNA was isolated

and prepared from roots as per the previous study[23]. RNA sequencing (RNA-seq) was performed using the Illumina sequencing platform at Biomarker Tech. Co. (Beijing, China). HISAT2[25] was used to map the clean reads to the *C. moschata* reference genome[26], and StringTie[27] was applied to assemble the mapped reads. Gene expression levels were quantified using the fragments per kilobase of transcript per million fragments (FPKM) mapped method. Differentially expressed genes (DEGs) were identified using DEseq2[28] with a threshold of false discovery rate (FDR) < 0.01 and $|\log_2$ FC (fold change)| ≥ 1. Transcripts were annotated using the following databases: NCBI non-redundant protein (NR), Swiss-Prot (a manually annotated, non-redundant protein database), Kyoto Encyclopedia of Genes and Genomes (KEGG), Gene Ontology (GO), Protein family (Pfam), euKaryotic Ortholog Groups (KOG), Clusters of Orthologous Groups of proteins (COG), and Evolutionary Genealogy of Genes: Non-supervised Orthologous Groups (eggNOG).

Quantitative real-time PCR (qRT-PCR) analysis

qRT-PCR was used to validate the RNA-seq results. The qualified RNA was transcribed into cDNA using the MonScript™ RTIII All-in-One Mix with dsDNase (Monad, Wuhan, China) based on the manufacturer's instructions. All samples were examined in triplicate. Gene-specific primers were designed using Primer Premier 5.0 software and are listed in Supplementary Table S1. qRT-PCR was performed on an Applied Biosystems 7500 thermocycler (Thermo Fisher Scientific, Waltham, MA, USA) using Super-Real PreMix Plus (SYBR Green) (TIANGEN Biotech Co., Beijing, China) according to the manufacturer's instructions. The expression levels of all target transcripts were normalized to the housekeeping gene *actin*[29].

Results

Performance of WCO39 seedlings under selenite treatment

As shown in Fig. 2a, the growth of WCO39 seedlings was significantly affected by different concentrations of selenite. In terms of plant growth phenotype, 2 μM selenite (Se2) significantly decreased the plant height by 8.90% (Fig. 2b), but had no significant effect on the hypocotyl diameter, leaf size, and petiole length compared to the control (0 μM selenite, Se0) (Fig. 2c–f). All these parameters were significantly reduced under the other concentrations of selenite, and the inhibitory effects became more pronounced as the concentration increased. Similarly, the fresh and dry weight of WCO39 seedling shoots and roots were not significantly affected under Se2 treatment, but decreased under higher concentrations of selenite, and the suppression intensified with increasing selenite concentration (Fig. 2g–j).

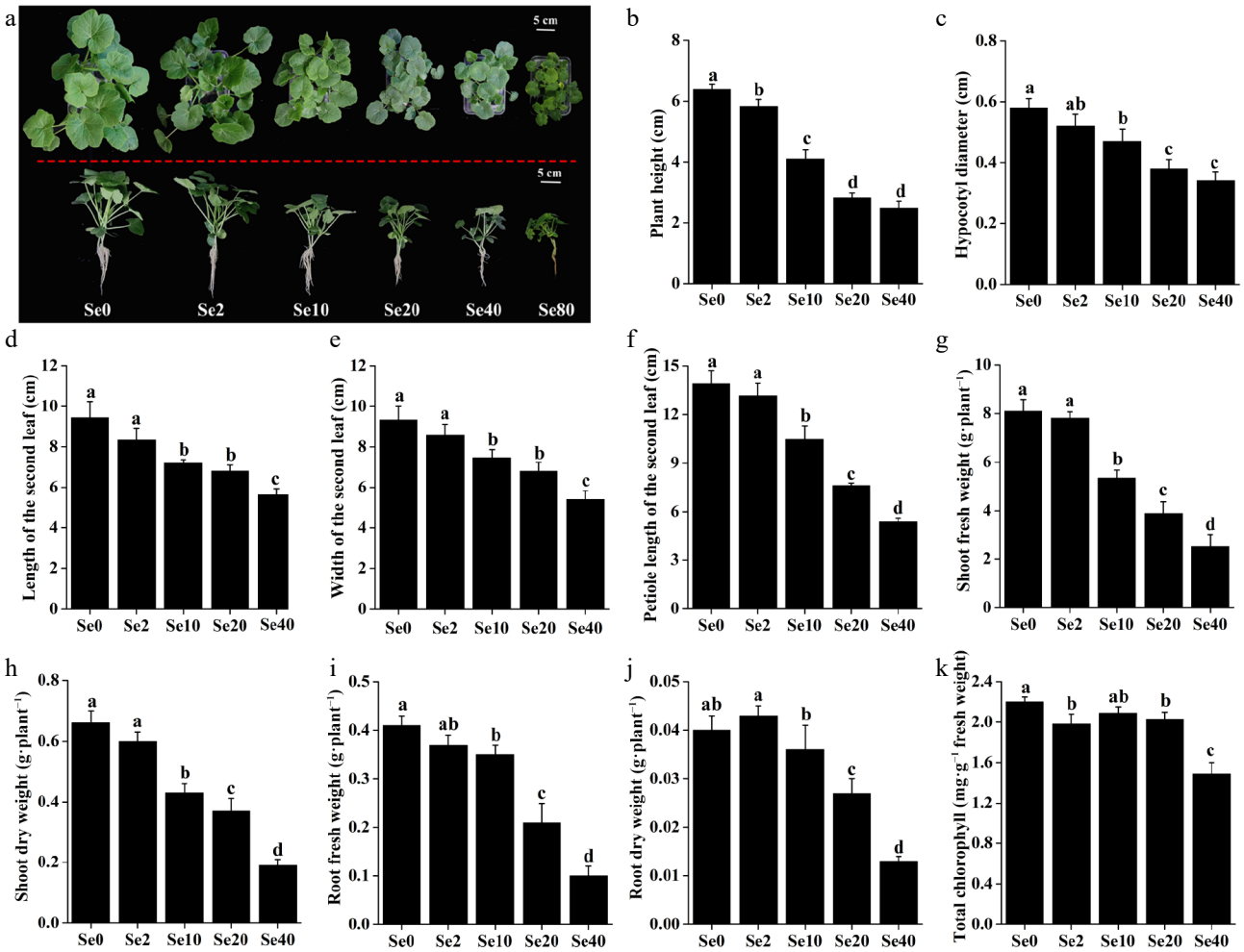

Fig. 2 Effects of different selenite concentrations on the growth of WCO39 seedlings. (a) Phenotypes after 10 d of selenite treatment with different selenite concentrations. The aerial and lateral views of WCO39 seedlings are shown. (b)–(k) Statistical analysis of different growth parameters resulting from different doses of selenite. Different small letters on the bars stand for significant differences at $p < 0.05$ according to Duncan's multiple scope tests. Se0, Se2, Se10, Se20, Se40, and Se80 represent 0, 2, 10, 20, 40, and 80 μM selenite treatment, respectively.

Se2 and Se20 treatments significantly reduced the content of total chlorophyll in WCO39 seedling leaves by 10% and 7.72%, respectively, compared to the control (Fig. 2k). It is worth noting that Se40 treatment decreased plant height by 61.41%, hypocotyl diameter by 41.38%, leaf length by 40.30%, leaf width by 42.12%, Petiole length by 61.37%, shoot fresh weight by 68.73%, shoot dry weight by 71.21%, root fresh weight by 75.61%, root dry weight by 67.50%, and total chlorophyll content by 32.27%, compared to Se0 treatment (Fig. 2), indicating the serious inhibition of plant growth under Se40 treatment. Moreover, the results showed that plants treated with 80 μM selenite (Se80) exhibited more pronounced symptoms of growth suppression, leaf chlorosis, and root necrosis (Fig. 2a). These results demonstrated the serious toxicity of high selenite concentrations to *C. moschata*.

Influence of selenite on the physiological parameters in WCO39 seedlings

$O_2^{\cdot-}$ accumulation in leaves was assessed and visualized by NBT staining (Fig. 3a). Compared to Se0 leaves, the intensity of the navy blue color (reflecting $O_2^{\cdot-}$ level) appeared reduced in Se2 leaves, while it was not significant in Se10 leaves. Leaves exposed to 20 and 40 μM selenite exhibited a more pronounced navy blue color compared to other treatments, indicating excessive $O_2^{\cdot-}$ accumulation in leaves under high selenite doses.

MDA content and REC in leaves were measured to assess the effects of selenite on membrane lipid peroxidation and permeability. The results showed that the MDA content and REC in Se2 leaves were similar to Se0, but increased rapidly under higher selenite concentrations (10 and 40 μM) (Figs 2c & 3b). Compared to Se0,

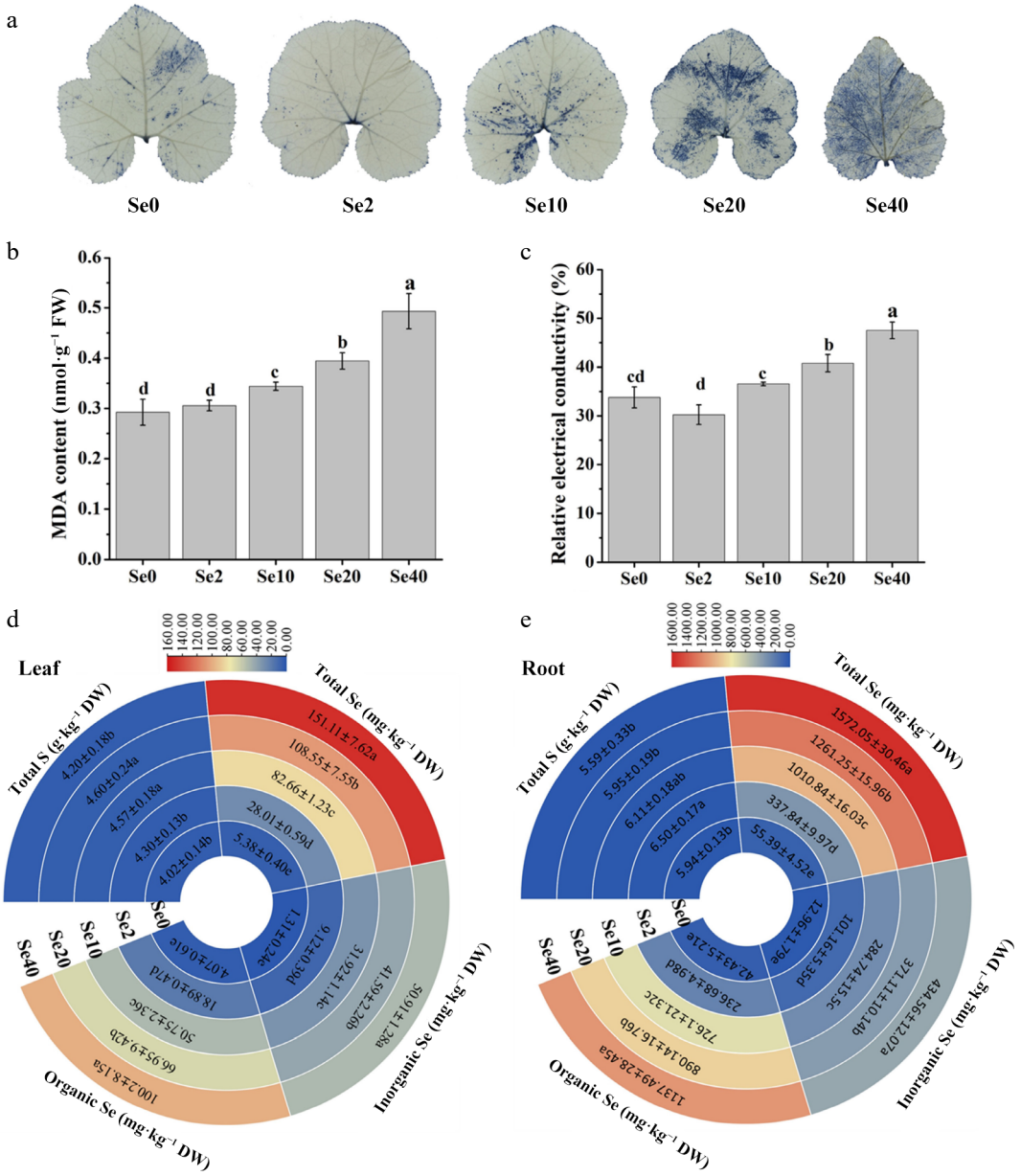

Fig. 3 Influence of selenite on various physiological parameters in WCO39 seedlings. (a) Accumulation of $O_2^{\cdot-}$ in leaves visualized by NBT staining. (b) MDA content. (c) Relative electrical conductivity. (d), (e) Heatmaps showing the content of total S, Se, inorganic Se, and organic Se in leaves and roots, respectively. Se0, Se2, Se10, Se20, Se40, and Se80 represent 0, 2, 10, 20, 40, and 80 μM selenite treatment, respectively. The data are shown as mean ± SD (n = 3). Different small letters on the bars and heatmaps stand for significant differences at $p < 0.05$ according to Duncan's multiple scope tests.

Se20 treatment increased MDA levels by approximately 35% and REC by 21%, while Se40 increased MDA by about 69% and REC by 57%. These results indicate that high doses of selenite induce membrane lipid peroxidation and increase membrane permeability in WCO39 leaves.

The effects of selenite treatment on S and Se contents in WCO39 seedlings were also analyzed (Fig. 3d, e). Compared to the control, S content was unaffected by Se2 in leaves, while it was increased slightly in roots. In contrast, both Se10 and Se20 treatments increased S content in leaves but not in roots. However, Se40 almost had no effect on the S contents in both leaves and roots compared with the control. In summary, selenite exerts a complex and tissue-specific influence on S content in *C. moschata* seedlings.

Total Se, inorganic Se, and organic Se contents in leaves and roots were also determined. As shown in Fig. 3d, e, all three Se fractions increased gradually and significantly with rising selenite concentration. Se accumulation in roots reached approximately 337.84, 1,010.84, 1,261.25, and 1,572.05 mg·kg^{-1} DW under Se2, Se10, Se20, and Se40, respectively. Corresponding Se levels in leaves were approximately 28.01, 82.66, 108.55, and 151.11 mg·kg^{-1} DW. Furthermore, the majority of accumulated Se was in organic forms, ranging from 61.40% to 67.44% in shoots and 70.06% to 72.36% in roots across the selenite concentrations tested (2–40 μM). These results indicate that *C. moschata* readily takes up selenite and converts it to organic Se forms.

RNA-seq analysis and identification of DEGs

To investigate the transcriptomic responses to selenite stress in WCO39, six cDNA libraries were prepared from three control (Se0-1, Se0-2, Se0-3) and three 40 μM selenite-treated (Se40-1, Se40-2, Se40-3) root samples. Sequencing and mapping results are summarized in Supplementary Table S2. An average of 43,611,804 clean reads per sample was obtained, with Q30 percentages ≥ 93.97%. Approximately 80.90% of clean reads mapped to the *C. moschata* reference genome, with > 78.40% uniquely mapped and < 2.41% multiply mapped. Pearson's correlation coefficients (R) between biological replicates exceeded 0.99 (Supplementary Fig. S2), and principal component analysis (PCA) revealed a clear separation between control and selenite treatment samples (Fig. 4a), confirming the reliability of the replicates in this study.

Comparing Se0 vs Se40 (with Se0 as control), the study identified 5,545 differentially expressed genes (DEGs), comprising 3,453 upregulated and 2,092 downregulated genes (Fig. 4b; Supplementary Fig. S3). This predominance of upregulated genes suggests that selenite-responsive genes were largely induced during the early stage of treatment. Hierarchical clustering of all DEGs showed tight grouping of the biological replicates within each treatment group (Fig. 4c). To validate the RNA-seq results, 20 DEGs with high expression levels in at least one group (FPKM > 10), including 15 upregulated and five downregulated genes, were selected for analysis by qRT-PCR. The qRT-PCR results strongly correlated with the RPKM values (R^2 = 0.92) (Fig. 4d), confirming the reliability of the identified DEGs.

KEGG pathway enrichment analysis of DEGs revealed their functional roles under selenite stress. The top 20 enriched pathways (smallest *q*-value) were shown in Fig. 4e. Notably, selenite-induced genes outnumbered inhibited genes in most enriched pathways (14/20), suggesting widespread pathway activation in response to selenite in WC40. These pathways included two related to plant hormone biosynthesis ('alpha-Linolenic acid metabolism' and 'Brassinosteroid biosynthesis'), four associated with stress response and defense ('Starch and sucrose metabolism', 'Phenylpropanoid biosynthesis', 'Glutathione metabolism', and 'MAPK signaling pathway-plant'), and one involved in membrane transport ('ABC transporters').

To further understand the functions of upregulated and downregulated genes, GO enrichment analysis was conducted separately on the 3,453 upregulated genes (Fig. 4f) and 2,092 downregulated genes (Fig. 4g). For the upregulated genes, 18, one and six significantly enriched terms were obtained in biological processes, cellular component and molecular function categories, respectively (Fig. 4f). Within BP, 15 terms were stress-related, including 'response to stress', 'response to toxic substance', 'response to reactive oxygen species', 'cellular response to stress', 'response to abiotic stimulus', and so on. The only enriched CC term was 'integral component of membrane' (744 genes). In MF, 'phenylalanine ammonia-lyase activity' (linked to phenylpropanoid metabolism) was the most enriched term. For the downregulated genes, significant enrichment was found for five BP, nine CC, and 19 MF terms (Fig. 4g). The most enriched BP term was 'plant-type cell wall organization'. One BP term related to ROS ('hydrogen peroxide catabolic process') was also enriched. In CC, downregulated genes were primarily associated with the cell nucleus ('nucleosome' and 'host cell nucleus'). Within MF, 'microtubule binding' was the most enriched term. These results suggest the complexity of selenite response in *C. moschata*.

Analysis of DEGs annotated to putative transporters

Based on NR database annotations, 162 DEGs were annotated as transporters and classified into 40 functional categories (Supplementary Fig. S4). ABC transporters constituted the largest proportion (about 17%) (Supplementary Fig. S4), with the majority (21/27) being upregulated by selenite treatment. Notably, seven ABC transporters, including *CmoCh11G001530*, *CmoCh11G001510*, *CmoCh11G001540*, *CmoCh05G007960*, *CmoCh14G009250*, *CmoCh07G000710* and *CmoCh01G011380*, exhibited both high expression (FPKM > 10) and significant upregulation (> 2-fold) under selenite stress (Fig. 5a; Supplementary Table S3). PHTs, which are reported to be involved in the uptake of selenite in plant roots[30], represented the second largest category (about 9%) (Supplementary Fig. S4), with most (10/14) showing upregulation under selenite treatment (Fig. 5b; Supplementary Table S3). Among them, *CmoCh12G006790* showed the highest expression level under selenite treatment, with a 4.56-fold increase compared to the control, and *CmoCh18G011500* exhibited the highest fold-change upregulation (14.79-fold) with high expression under selenite treatment. Additionally, two PHTs (*CmoCh14G018470* and *CmoCh06G013160*) were downregulated > 4-fold by selenite treatment.

The DEGs encoding sulfate transporters (SULTRs) were also examined due to their implication in selenate transport[30]. Five differentially expressed SULTRs were identified, three of which (*CmoCh19G002880*, *CmoCh14G017790*, and *CmoCh08G003200*) were suppressed by selenite treatment (Fig. 5c; Supplementary Table S3). Notably, *CmoCh10G006430* was significantly upregulated (2.95-fold) and highly expressed under selenite treatment.

Analysis of DEGs related to Ca^{2+} influx, sensor, and efflux

As shown in Fig. 5d and Supplementary Table S4, three DEGs were annotated as encoding cyclic nucleotide-gated ion channel (CNGC), and two of them showed significant upregulation under selenite stress. Additionally, selenite treatment resulted in differential expression of two calmodulin genes (CaMs), 18 CaM-like protein genes (CMLs), ten calcium-dependent protein kinase genes (CDPKs), and three calcineurin B-like protein genes (CBLs). Among these, the majority (both CaMs, 16 of 18 CMLs, nine of ten CDPKs, and two of three CBLs) exhibited significantly higher expression compared to

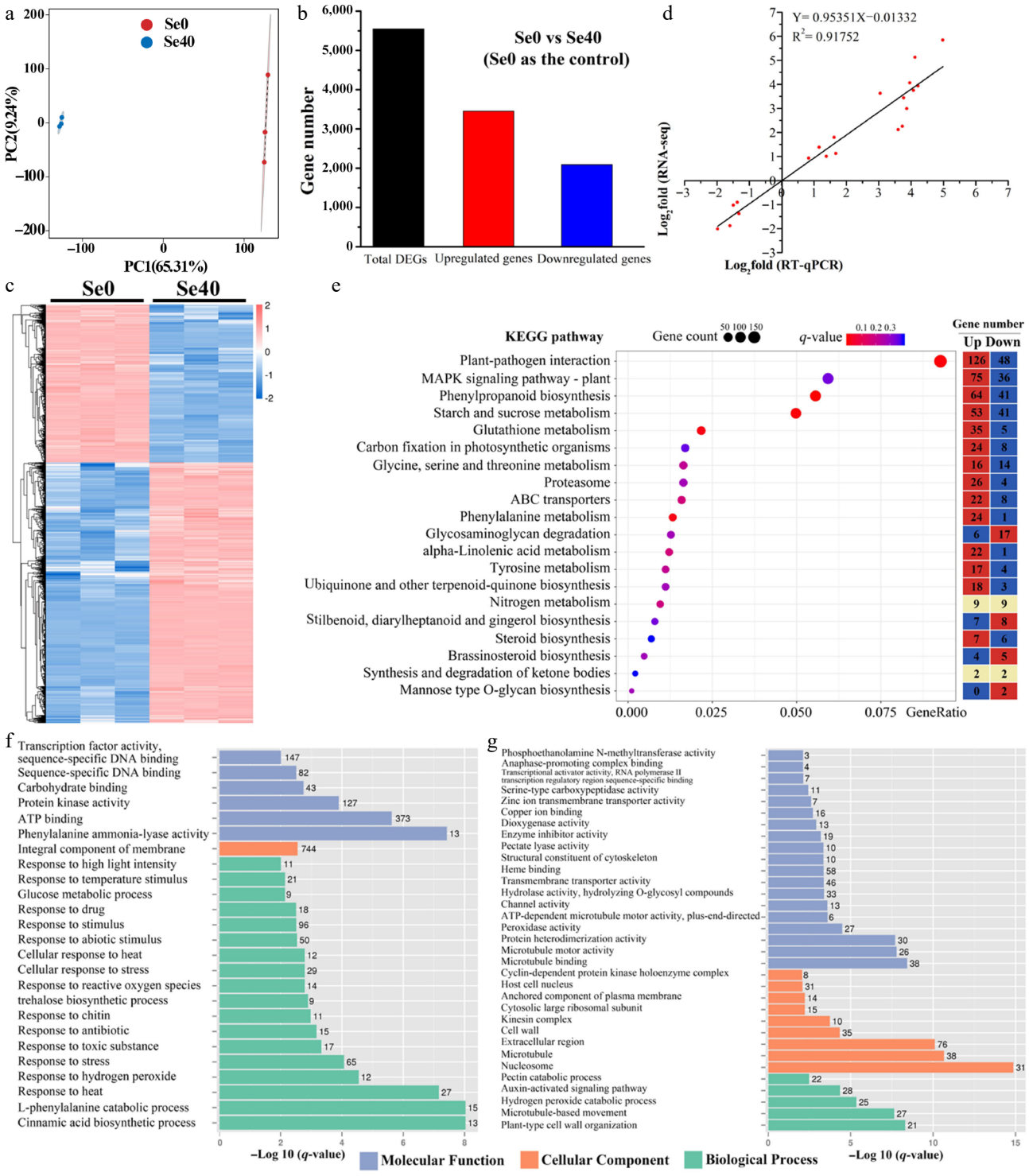

Fig. 4 Analysis of differentially expressed genes (DEGs) identified in Se0 vs Se40 comparison. (a) Principal component analysis (PCA) analysis. (b) Number of DEGs in Se0 vs Se40. (c) Heatmap showing the hierarchical clustering of DEGs. Both the rows and the columns are scaled by normalization. (d) Correlation analysis between the RNA-seq and qRT-PCR results. The abscissa (X-Ais) and ordinate (Y-Ais) quantitatively represent the Log2-transformed fold-change values (Se40/Se0) derived from RNA-seq and qRT-PCR analyses, respectively. (e) KEGG pathway enrichment analysis of DEGs. The topmost enriched 20 KEGG pathways with the lowest *q*-values are shown. Gene ratio refers to the ratio of the DEGs to the total number of annotated genes in each pathway. The heatmap on the right side shows the number of upregulated and downregulated genes in each KEGG pathway. (f), (g) GO enrichment analysis of the upregulated and downregulated genes, respectively. The topmost enriched GO terms under the three main GO categories are displayed.

the control (Fig. 5d; Supplementary Table S4). Notably, four CMLs (*CmoCh10G000650*, *CmoCh04G021950*, *CmoCh11G00042*, *CmoCh11G000420*) and one CBL (*CmoCh19G003980*) were upregulated > 10-fold by selenite. Furthermore, the CDPK-encoding gene *CmoCh03G000720* displayed about 3.2-fold upregulation (Fig. 5d; Supplementary Table S4). Four DEGs annotated as Ca^{2+}-ATPases and one as a Ca^{2+}/H^{+} exchanger were also identified, all of which responded positively to selenite treatment (Fig. 5d; Supplementary Table S4). Collectively, these results suggest that selenite activates multiple components of calcium signaling pathways in WCO39 seedlings.

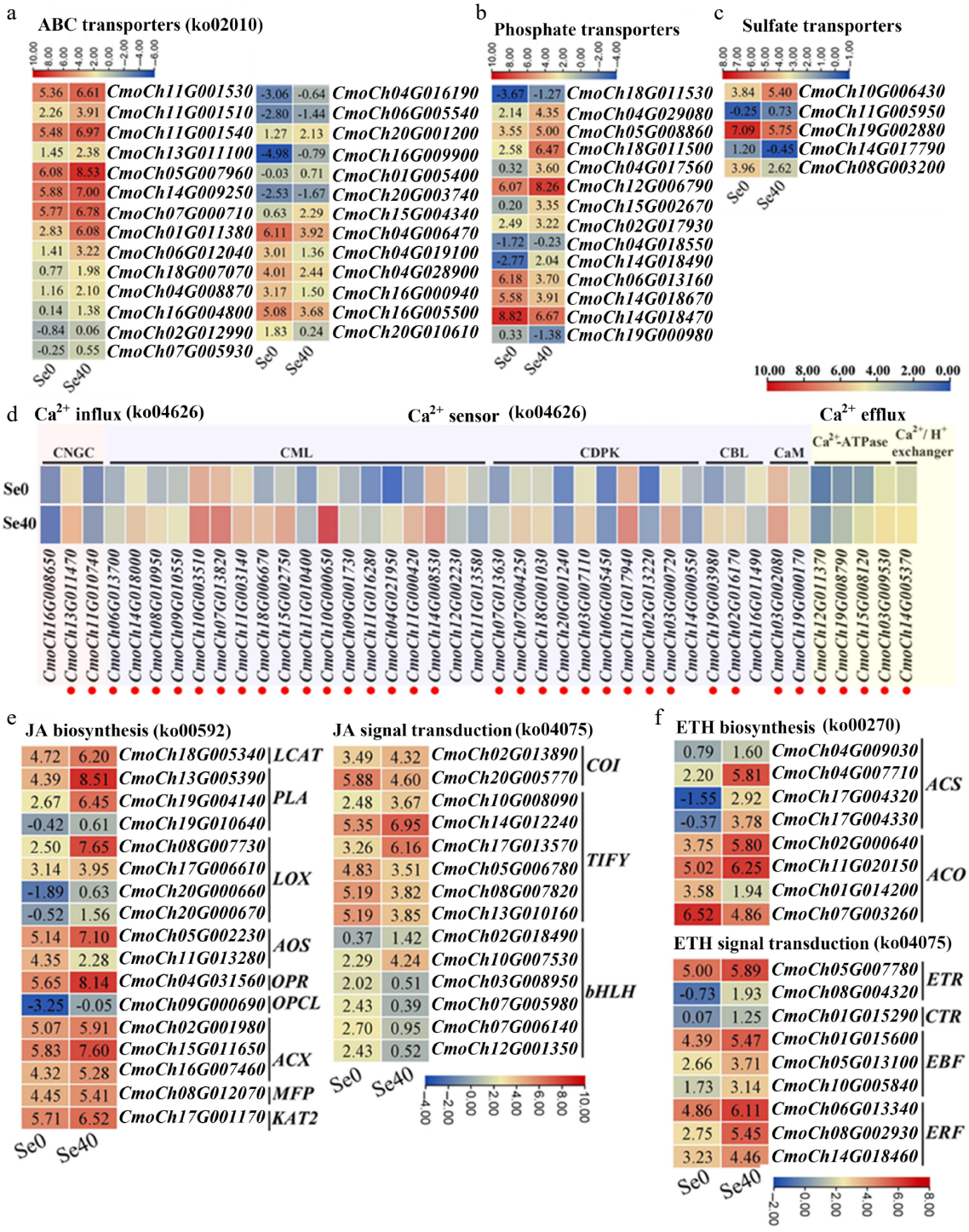

Fig. 5 Heatmaps showing DEGs involved in several important pathways. (a)–(c) ABC transporters, phosphate transporters, and sulfate transporters, respectively. Upregulated genes are marked in red. (d) Ca^{2+} influx, sensors, and efflux. CNGC: cyclic nucleotide-gated ion channel; CaM, calmodulin; CML: CaM-like protein; CBL: calcineurin B-like protein; CDPK: calcium-dependent protein kinase. (e), (f) DEGs related to the biosynthesis and signal transduction of JA and ETH, respectively. LCAT: lecithin-cholesterol acyltransferase; PLA: phospholipas; LOX: lipoxygenase; AOS: allene oxide synthase; OPR: oxophytodienoate reductase; ACX: acyl-coenzyme A oxidase; MFP: multifunctional protein; OPCL: 4-coumarate—CoA ligase; KAT: ketoacyl-CoA thiolase; COI: coronatine-insensitive protein; bHLH: basic helix-loop-helix protein; ACS: 1-aminocyclopropane-1-carboxylate synthase; ACO: 1-aminocyclopropane-1-carboxylate oxidase; ETR: ethylene receptor; CTR: constitutive triple response protein; EBF: EIN3-binding F-box protein; ERF: ethylene-responsive transcription factor. Some pathways have been listed with their corresponding KEGG pathway ID numbers behind them. The Log_2 (FPKM) for each gene in different samples is shown in the appropriate grid.

Analysis of DEGs related to biosynthesis and signal transduction of jasmonate and ethylene

Seventeen DEGs associated with jasmonate (JA) biosynthesis and 14 DEGs involved in JA signal transduction were identified (Fig. 5e; Supplementary Table S5). Sixteen of the 17 putative JA biosynthesis genes were upregulated by selenite treatment. These included genes encoding: LCAT (*CmoCh18G005340*), PLA (*CmoCh13G005390*, *CmoCh19G004140*, *CmoCh19G010640*), LOX (*CmoCh08G007730*,

CmoCh17G006610, *CmoCh20G000660*, *CmoCh20G000670*), AOS (*CmoCh05G002230*), OPR (*CmoCh04G031560*), OPCL (*CmoCh09G000690*), ACX (*CmoCh02G001980*, *CmoCh15G011650*, *CmoCh16G007460*), MFP (*CmoCh08G012070*), and KAT (*CmoCh17G001170*). For the 14 putative JA signal transduction genes, only six were upregulated. These comprised one COI1 (*CmoCh02G013890*), three TIFYs (*CmoCh10G008090*, *CmoCh14G012240*, *CmoCh17G013570*), and two bHLHs (*CmoCh02G018490*, *CmoCh10G007530*), suggesting complex regulation of JA biosynthesis and signaling pathways by selenite treatment.

Additionally, eight DEGs involved in ethylene (ETH) biosynthesis were identified. Most (6/8) were significantly upregulated by selenite treatment, particularly *CmoCh04G007710*, *CmoCh17G004320*, *CmoCh17G004330*, and *CmoCh02G000640*, exhibiting fold-change increases of about 12.13, 22.10, 17.81, and 4.14, respectively (Fig. 5f; Supplementary Table S5). Nine DEGs involved in ETH signal transduction, encompassing two ETRs, one CTR1-like, three EBFs, and three ERFs, were also identified. All were significantly upregulated in response to selenite treatment (Fig. 5f; Supplementary Table S5), indicating activation of both ETH biosynthesis and signaling pathways in WCO39 seedlings by selenite treatment.

Analysis of DEGs related to Se assimilation and the MAPK signaling pathway

Nine DEGs involved in Se assimilation were identified (Table 1; Supplementary Table S6). Seven were significantly upregulated, including genes encoding APS (*CmoCh14G017980*), APK (*CmoCh16G003340*), APR (*CmoCh06G017430*), SO (*CmoCh15G000800*), GR (*CmoCh14G019350*), and CS (*CmoCh10G011250*, *CmoCh10G011260*). Notably, *CmoCh10G011250* showed both the highest upregulation (about 3.08-fold) and the highest expression abundance under selenite treatment, suggesting its importance for Se assimilation in WCO39 roots.

Additionally, 11 DEGs associated with the MAPK cascade were regulated by selenite treatment (Table 1; Supplementary Table S6). These included four CmoMAPKs (*CmoCh01G005840*, *CmoCh04G000390*, *CmoCh18G000490*, *CmoCh13G010340*), one CmoMAPKK (*CmoCh12G013530*), and six CmoMAPKKKs (*CmoCh07G007160*, *CmoCh19G009390*, *CmoCh01G011670*, *CmoCh02G001800*, *CmoCh15G007330*, *CmoCh17G002450*). All four CmoMAPKs were upregulated, especially *CmoCh01G005840*, which exhibited the highest fold-change increase (about 2.24-fold) and the highest expression abundance under selenite treatment. Expression of the CmoMAPKK was increased about 2-fold by selenite treatment. Most CmoMAPKKKs (4/6) were significantly upregulated, particularly *CmoCh07G007160* and *CmoCh15G007330*, with fold-change increases of about 2.73 and 2.38, respectively.

Analysis of DEGs related to the GSH cycle, ASA-GSH cycle

Three DEGs (*CmoCh07G005120*, *CmoCh01G016350,* and *CmoCh14G019720*) involved in the glutathione (GSH) cycle were significantly upregulated by selenite treatment (Fig. 6; Supplementary Table S7). Nine genes associated with the ascorbate (ASA)-GSH cycle also responded to selenite treatment. Eight of these (excluding *CmoCh15G0113160*) were significantly upregulated, including genes encoding: GR (*CmoCh14G019350*), GPX (*CmoCh15G012860*), MDHAR (*CmoCh14G002840*), APX (*CmoCh20G004910*), Cu/Zn-SOD (*CmoCh10G011710*) and DHAR (*CmoCh04G002430*, *CmoCh04G002440,* and *CmoCh04G002450*) (Fig. 6; Supplementary Table S7). Additionally, 14 glutathione S-transferase (GST)-encoding DEGs were significantly upregulated by selenite treatment. Eight of them exhibited particularly strong induction, including *CmoCh16G005000* (8.80-fold), *CmoCh07G010750* (5.80-fold), *CmoCh03G003940* (14.58-fold), *CmoCh16G004990* (8.80-fold), *CmoCh03G003950* (15.46-fold), *CmoCh07G010720* (17.32-fold), *CmoCh16G005010* (11.59-fold), and *CmoCh06G003370* (13.90-fold). These results revealed the activation of both glutathione and ASA-GSH cycles in *C. moschata* seedlings under 40 μM selenite treatment.

Analysis of DEGs related to melatonin biosynthesis and the influence of exogenous melatonin treatment on selenite stress

Caffeic acid 3-O-methyltransferase (COMT) catalyzes the final step of MT biosynthesis in *Arabidopsis*, converting N-acetylserotonin to MT[31]. Five COMT-encoding DEGs significantly upregulated by selenite treatment were identified (Fig. 7a; Supplementary Table S8), meaning selenite activates COMT expression in *C. moschata* seedlings.

Given melatonin's established roles in abiotic stress resistance[16], the effect on selenite-stressed seedlings was examined. The MT-treated group (Se40MT100) showed significantly improved

Table 1. List of genes related to selenium assimilation and MAPK cascade.

Gene ID	Gene description	Gene synonym	Se0_FPKM	Se40_FPKM	log2 (fold change)
CmoCh01G020230	ATP sulfurylase 2	CmoAPS	2.86	0.85	−1.47
CmoCh14G017980	ATP sulfurylase 1		2.80	4.96	1.09
CmoCh16G003340	Adenylyl-sulfate kinase 3	CmoAPK	2.13	5.31	1.58
CmoCh06G017430	5'-adenylylsulfate reductase 5	CmoAPR	22.22	40.04	1.12
CmoCh15G000800	Sulfite oxidase	CmoSO	10.46	25.85	1.58
CmoCh11G008630	Sulfite reductase	CmoSiR	38.88	14.97	−1.10
CmoCh10G011250	Cysteine synthase	CmoCS	37.43	115.32	1.90
CmoCh10G011260	Cysteine synthase		1.69	3.08	1.14
CmoCh14G019350	Glutathione reductase	CmoGR	17.50	44.68	1.63
CmoCh01G005840	Mitogen-activated protein kinase 3	CmoMAPK	92.46	207.21	1.44
CmoCh04G000390	Mitogen-activated protein kinase 9		21.45	38.13	1.10
CmoCh18G000490	Mitogen-activated protein kinase 9		3.04	6.83	1.44
CmoCh13G010340	Mitogen-activated protein kinase 9		0.38	1.98	2.67
CmoCh12G013530	Mitogen-activated protein kinase kinase 1	CmoMAPKK	13.07	25.41	1.23
CmoCh07G007160	Mitogen-activated protein kinase kinase kinase 17	CmoMAPKKK	4.45	12.19	1.73
CmoCh19G009390	Mitogen-activated protein kinase kinase kinase 17		0.51	1.21	1.51
CmoCh01G011670	Mitogen-activated protein kinase kinase kinase 18		19.82	4.70	−1.80
CmoCh02G001800	Mitogen-activated protein kinase kinase kinase 18		0.20	1.29	2.87
CmoCh15G007330	Mitogen-activated protein kinase kinase kinase 1		8.21	19.54	1.52
CmoCh17G002450	Mitogen-activated protein kinase kinase kinase		7.65	1.68	−1.91

The false discovery rate (FDR) values for all genes are less than 0.001.

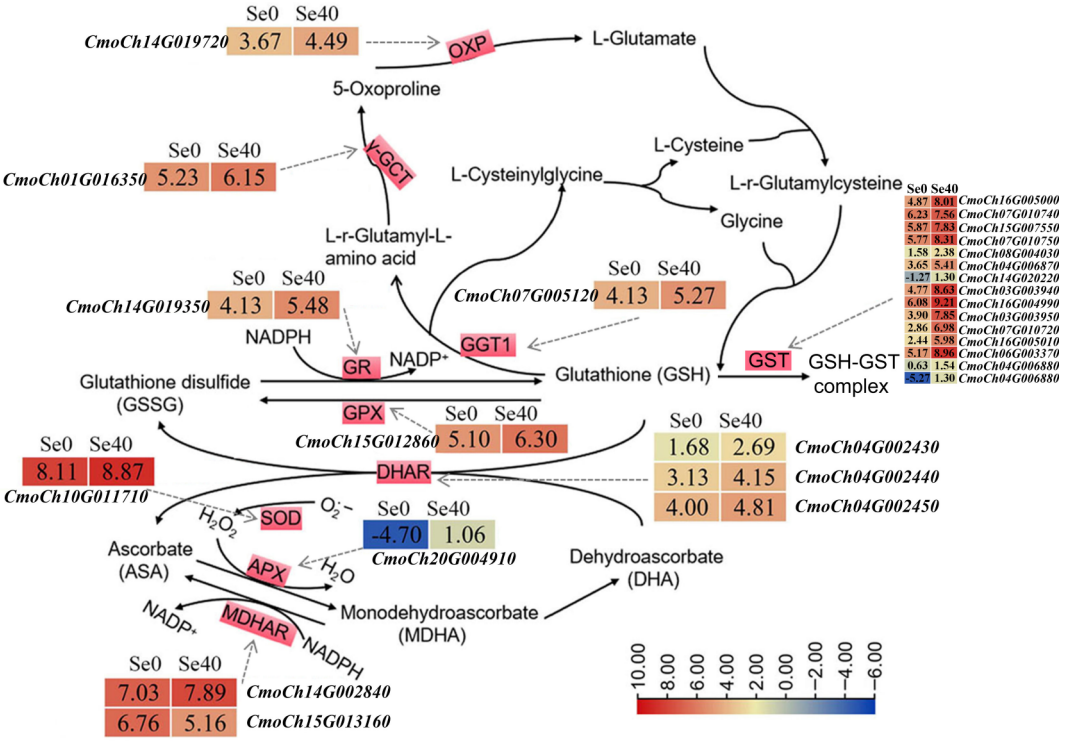

Fig. 6 DEGs related to GSH and ASA-GSH cycles. The solid arrows indicate the substrates and products of the metabolic reaction. The dotted arrows represent the enzymes encoded by the corresponding DEGs identified in Se0 vs Se40 (Se0 as the control). The heatmaps represent the corresponding expression levels of DEGs, and the Log_2 (FPKM) for each gene is shown in the appropriate grid.

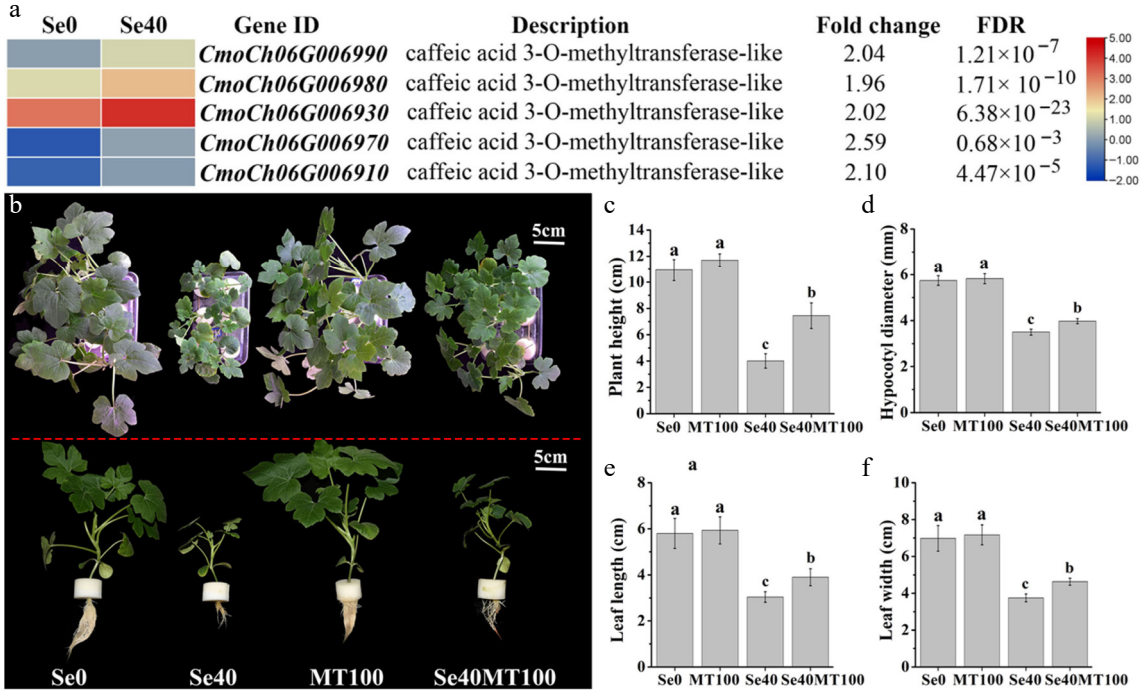

Fig. 7 Analysis of DEGs involved in melatonin biosynthesis and the influence of exogenous melatonin treatment on selenite stress. (a) Heatmap showing DEGs annotated to encoding caffeic acid 3-O-methyltransferase. The Log_2 (FPKM) for each gene is used to generate this heatmap. (b) Phenotypes of WCO39 seedlings under different treatments. (c)–(f) Statistical analysis of different growth indicators. Se0 represents normal seedlings; Se40 represents seedlings irrigated with 40 μM selenite; MT100 represents seedlings grown in normal culture with foliar application of 100 μM melatonin; Se40MT100 represents seedlings treated with 40 μM selenite and also sprayed with 100 μM melatonin. The data are shown as mean ± SD (n = 3). Different small letters on the bars stand for significant differences at $p < 0.05$ according to Duncan's multiple scope tests.

growth versus selenite-only controls (Se40) (Fig. 7b–f). This mitigation of selenite toxicity was evident by increased plant height, hypocotyl diameter, and leaf area (Fig. 7c–f), indicating melatonin's protective role against selenite stress in *C. moschata* seedlings.

Discussion

In plants, Se has been reported to be beneficial for growth and biomass accumulation at low concentrations, but toxic at higher

levels, leading to growth retardation, reduced biomass, chlorosis, and ultimately plant death[5,7,11]. To date, the effects of Se on pumpkin growth have not been reported. In this study, *C. moschata* seedlings were treated with different concentrations of selenite, a dominant bioavailable form of Se in soil[17]. Results indicated that 2 μM selenite had only a slight effect on *C. moschata* seedling growth. However, moderate concentrations (10–20 μM) significantly retarded growth and increased S content in shoots, consistent with previous studies in cucumber[32] and *Arabidopsis*[33]. High selenite concentrations impaired growth and physiology in *C. moschata*: 40 μM significantly inhibited growth and reduced chlorophyll content, while 80 μM induced severe phytotoxicity, characterized by leaf chlorosis and root necrosis. Similarly, cucumber exhibited significant phytotoxic effects at selenite concentrations exceeding 20 μM[32]. These results show a dose-dependent toxic effect on *C. moschata* under selenite treatment and underscore the need to identify optimal Se concentrations for cucurbit crops during biofortification.

Selenite absorbed by roots is rapidly converted to organic forms within roots, with limited translocation to shoots[34]. Se accumulation occurs predominantly in organic forms, as observed in rice[35]. Similarly, the results showed that organic Se levels in both leaves and roots were significantly higher than inorganic Se levels across selenite treatments, with the majority of Se accumulating in roots. Furthermore, Se content in both shoots and roots of *C. moschata* seedlings exhibited a dose-dependent response to selenite. Transportation of selenite across the root plasma membrane is mainly mediated by PHTs[17]. In rice, overexpression of *OsPHT2* increased selenite uptake, while mutants exhibited decreased uptake[36], confirming the importance of PHTs for selenite absorption in plants. In this study, several PHTs were highly upregulated in response to selenite treatment, likely facilitating selenite uptake in *C. moschata*. Inostroza-Blancheteau et al.[37] and Cao et al.[38] reported that SULTRs can be activated by selenite in plant roots. In this study, two significantly upregulated SULTRs belonging to the SULTR3;5 subfamily in *C. moschata* were identified. According to previous studies, SULTR3;5 colocalizes with SULTR2;1 in plant root xylem[39], and SULTR2;1 facilitates sulfate and selenate translocation from roots to shoots[17]. This suggests that high expression of SULTR3;5 in *C. moschata* roots may contribute to selenite translocation to shoots. Furthermore, these findings support a role for ABC transporters in Se accumulation[12,40], as numerous ABC transporter genes were differentially expressed, with the majority significantly upregulated by selenite treatment.

Due to the high chemical similarity between Se and S, Se typically enters the S metabolic pathway in plants, forming various Se compounds[17]. Sulfite oxidase (SO) catalyzes the oxidation of sulfite to sulfate in plants[41]. It was found that the *SO* gene *CmoCh15G 000800* was significantly upregulated by selenite treatment, which should contribute to the oxidation of selenite in *C. moschata* roots. This hypothesis is further supported by the significant upregulation of genes encoding APS, APK, and APR, which are involved in selenate reduction to selenite in plants[17]. Several studies report that selenite can be non-enzymatically reduced to selenide by GSH in plants, and glutathione reductase (GR) plays a key role in this pathway[17]. This study identified one GR-encoding gene, *CmoCh 14G019350*, whose expression was greatly upregulated by selenite treatment in *C. moschata*. CS exhibits a higher affinity for selenide than sulfide and catalyzes its conversion to SeCys[7]. Two *CS* genes were significantly upregulated, implying their importance for SeCys synthesis in *C. moschata*.

Calcium (Ca^{2+}) is a ubiquitous second messenger that plays critical roles in plant responses to abiotic stresses[42]. The results revealed that selenite stress significantly upregulated CNGC-encoding genes. CNGCs act as 'on' components of Ca^{2+} signaling, mediating stress-induced Ca^{2+} influx[42], suggesting that selenite induces Ca^{2+} uptake and activates Ca^{2+} signaling in *C. moschata*. As expected, numerous genes encoding calcium sensors, including CaMs, CMLs, CDPKs, and CBLs[43], showed altered expression under selenite treatment, with most being upregulated. However, Rao et al.[12] observed the downregulation of *CDPKs* under selenate treatment in *Cardamine violifolia*. These contrasting results may stem from differences in plant species, Se forms (selenite vs selenate), concentration, or treatment duration. It is reported that Ca^{2+} signaling induces respiratory burst oxidase homolog (RBOH)-mediated ROS production, which further promotes Ca^{2+} influx by activating calcium-permeable ion channels[44]. In this study, two upregulated *RBOHs* were identified, both of which exhibited significantly higher expression under both control and selenite treatment conditions, implying their activation by Ca^{2+} signaling during selenite exposure in *C. moschata*. This observation aligns with reports that selenium acts as a pro-oxidant, generating ROS at high concentrations in plants[7]. Ca^{2+}-ATPase and Ca^{2+}/H^{+} exchangers are mainly membrane proteins responsible for Ca^{2+} efflux to maintain cellular Ca^{2+} homeostasis under abiotic stresses[42,45]. The study found three Ca^{2+}-ATPase genes and two Ca^{2+}/H^{+} exchanger genes significantly upregulated in selenite-treated *C. moschata*. This enhanced efflux activity suggests excessive Ca^{2+} accumulation occurs under selenite stress. Collectively, these DEGs related to Ca^{2+} influx, sensing, and efflux reflected that Ca^{2+} signaling should be involved in plant response to selenite treatment.

Se toxicity primarily stems from ROS-mediated oxidative stress in plants[7]. The results revealed excessive $O_2^{\cdot-}$ accumulation in leaves of WCO39 seedlings treated with high selenite doses (> 20 μM). GSH serves as a crucial non-enzymatic antioxidant for ROS detoxification and redox signaling[46]. Elevated GSH levels in Se-tolerant plants and their depletion-linked ROS accumulation[15] underscore GSH's importance in Se stress adaptation. GGT, GCT, and OXP enzymes are involved in GSH degradation in plants[47]. Thus, significantly elevated expressions of *GGT*, *GCT*, and *OXP* genes in response to selenite imply enhanced GSH metabolism under selenite stress in *C. moschata*. The ascorbate-glutathione (AsA-GSH) pathway has been well documented in ROS scavenging[48]. Upregulation of *GR*, *GPX*, *DHAR*, *APX*, and *MDHAR* genes under selenite treatment indicates that the AsA-GSH cycle should contribute to protecting cells from oxidative damage under selenite stress in *C. moschata*. Notably, all 14 GST-encoding DEGs responded positively to selenite. Similar upregulation of GSTs was reported in tea roots under selenite treatment[40]. Since GSTs catalyze GSH conjugation to electrophilic substrates, mitigating oxidative burst[49], GST-mediated metabolism likely contributes to the survival of *C. moschata* from high concentration selenite stress.

The MAPK cascade—comprising MAPKKK, MAPKK, and MAPK components—is a conserved signaling pathway regulating plant adaptation to environmental stresses, and it can be activated by abiotic stress-induced Ca^{2+} and ROS signals[50,51]. In *Arabidopsis*, MAPKs promote ETH biosynthesis by phosphorylating ACS (the rate-limiting enzyme of ETH biosynthesis) and upregulating *ACS* expression[52,53]. Suppression of *MAPKs* resulted in decreased expression of JA biosynthesis and signaling genes[54,55]. Hoewyk et al.[33] reported reduced Se tolerance in ETH/JA-response-deficient *Arabidopsis* mutants. While Se regulates ROS-mediated MAPK pathways in mammals[56], the relationship between Se and the MAPK cascade in plants remains poorly characterized. Here, selenite treatment significantly elevated expressions of both MAPK cascade genes and ETH/JA biosynthesis/signaling genes, suggesting MAPK

cascade-mediated regulation of ETH and JA pathways contributes to selenite toxicity responses in *C. moschata*.

Melatonin (MT) alleviates ROS-mediated oxidative stress in plants[57]. Several studies reveal the relationships between Se stress and MT. For example, Se exposure induces MT synthesis-related genes in tomato[58]. Exogenous MT enhances grape growth under Se stress[14]. These results revealed that selenite treatment significantly upregulated multiple *COMTs* in *C. moschata*. The enzymes encoded by *COMTs* catalyze the conversion of N-acetylserotonin to MT, a pivotal step in MT biosynthesis[31]. Exogenous MT application alleviated selenite-induced growth inhibition in *C. moschata* seedlings, suggesting that *COMT*-mediated MT synthesis contributes to *C. moschata*'s selenite stress response.

Conclusions

The narrow threshold between Se bioavailability and phytotoxicity complicates agricultural applications. Understanding Se effects on Cucurbita moschata seedlings is essential, as this species serves both as a health food and a rootstock for other cucurbits. Treatment with different selenite concentrations revealed that selenite induced dose-dependent Se accumulation in both *C. moschata* shoots and roots. It was also found that high selenite concentrations (> 40 μM) induced severe $O_2^{\cdot-}$ accumulation, growth arrest, and visible toxicity symptoms (leaf chlorosis, root necrosis) during *C. moschata* seedling growth. Notably, transcriptome analysis indicated that 40 μM selenite could induce expressions of several MT biosynthesis genes, and exogenous MT application alleviated growth inhibition under selenite stress, demonstrating the role of MT in selenite stress amelioration. Besides, many genes related to Ca^{2+} signaling, ETH and JA signaling, antioxidant defense systems, MAPK cascades, transporters related to selenite absorption, and selenite assimilation genes were activated by selenite treatment, suggesting their involvement in selenite response in *C. moschata* seedlings. Collectively, these findings advance the understanding of selenite response mechanisms in cucurbits, providing genetic targets and molecular insights for breeding Se-enriched pumpkin varieties with enhanced stress resilience.

Author contributions

The authors confirm contributions to the paper as follows: study conception and design: Wang Y, Sun S, Zhu L; data collection: Wang Y, Wang L, Liu W, Wang J; analysis and interpretation of results: Wang Y, Zhang T, Li Y, Mushtaq N; draft manuscript preparation: Wang Y, Mushtaq N, with contributions from Li Y, Zhu L, Yang L. All authors reviewed the results and approved the final version of the manuscript.

Data availability

RNA-seq data for this study are available in the National Center for Biotechnology Information (NCBI) repository, Bioproject: PRJNA1091146.

Acknowledgments

This research was supported by Henan Provincial Science and Technology Key Project (Grant No. 232102110232), and Henan Provincial Natural Science Foundation General Program (Grant No. 242300421322). The authors express their special gratitude to all the funding sources for the financial assistance.

Conflict of interest

The authors declare that they have no conflict of interest. The research was conducted in the absence of any commercial or financial relationships that could be construed as a potential conflict of interest. Henan Zhongwei Chunyu Plant Nutrition Co., Ltd. had no any involvement in the study.

Supplementary information accompanies this paper at (https://www.maxapress.com/article/doi/10.48130/vegres-0025-0026)

Dates

Received 1 May 2025; Revised 26 June 2025; Accepted 14 July 2025; Published online 12 September 2025

References

1. Aziz A, Noreen S, Khalid W, Ejaz A, Faiz ul Rasool I, et al. 2023. Pumpkin and pumpkin byproducts: phytochemical constitutes, food application and health benefits. *ACS Omega* 8(26):23346−57
2. Tangjaidee P, Swedlund P, Xiang J, Yin H, Quek SY. 2022. Selenium-enriched plant foods: selenium accumulation, speciation, and health functionality. *Frontiers in Nutrition* 9:962312
3. Winkel LHE, Johnson CA, Lenz M, Grundl T, Leupin OX, et al. 2012. Environmental selenium research: from microscopic processes to global understanding. *Environmental Science & Technology* 46(2):571−79
4. Qu L, Xu J, Dai Z, Elyamine AM, Huang W, et al. 2023. Selenium in soil-plant system: transport, detoxification and bioremediation. *Journal of Hazardous Materials* 452:131272
5. Abdullah, Wani KI, Hayat K, Naeem M, Aftab T. 2025. Multifaceted role of selenium in plant physiology and stress resilience: a review. *Plant Science* 355:112456
6. Qin X, Wang Z, Lai J, Liang Y, Qian K. 2025. The synthesis of selenium nanoparticles and their applications in enhancing plant stress resistance: a review. *Nanomaterials* 15(4):301
7. Gupta M, Gupta S. 2016. An overview of selenium uptake, metabolism, and toxicity in plants. *Frontiers in Plant Science* 7:2074
8. Yang X, Liao X, Yu L, Rao S, Chen Q, et al. 2022. Combined metabolome and transcriptome analysis reveal the mechanism of selenate influence on the growth and quality of cabbage (*Brassica oleracea* var. *capitata* L.). *Food Research International* 156:111135
9. Amerian M, Palangi A, Gohari G, Ntatsi G. 2024. Enhancing salinity tolerance in cucumber through Selenium biofortification and grafting. *BMC Plant Biology* 24(1):24
10. Yu Y, Yang Y, Guo Y, Pan M, Hao W. 2025. Exogenous selenium enhances cadmium stress tolerance by improving physiological characteristics of *Artemisia argyi* seedlings. *Scientific Reports* 15(1):3450
11. Ikram S, Li Y, Lin C, Yi D, Heng W, et al. 2024. Selenium in plants: a nexus of growth, antioxidants, and phytohormones. *Journal of Plant Physiology* 296:154237
12. Rao S, Yu T, Cong X, Lai X, Xiang J, et al. 2021. Transcriptome, proteome, and metabolome reveal the mechanism of tolerance to selenate toxicity in *Cardamine violifolia*. *Journal of Hazardous Materials* 406:124283
13. Wang J, Liu L, Zhang H, Zhang D, Dai Z, et al. 2024. Exogenous indole-3-acetic acid promotes the plant growth and accumulation of selenium in grapevine under selenium stress. *BMC Plant Biology* 24(1):426
14. Wang J, Lu Y, Xing S, Yang J, Liu L, et al. 2024. Transcriptome analysis reveals the promoting effects of exogenous melatonin on the selenium uptake in grape under selenium stress. *Frontiers in Plant Science* 15:1447451
15. Grant K, Carey NM, Mendoza M, Schulze J, Pilon M, et al. 2011. Adenosine 5'-phosphosulfate reductase (APR2) mutation in *Arabidopsis* implicates glutathione deficiency in selenate toxicity. *Biochemical Journal* 438(2):325−35
16. Sun C, Liu L, Wang L, Li B, Jin C, et al. 2021. Melatonin: a master regulator of plant development and stress responses. *Journal of Integrative Plant Biology* 63(1):126−45
17. Zhang L, Chu C. 2022. Selenium uptake, transport, metabolism, reutilization, and biofortification in rice. *Rice* 15(1):30

18. Lintschinger J, Fuchs N, Moser J, Kuehnelt D, Goessler W. 2000. Selenium-enriched sprouts. A raw material for fortified cereal-based diets. *Journal of Agricultural and Food Chemistry* 48(11):5362−68
19. Zhu YG, Pilon-Smits EAH, Zhao FJ, Williams PN, Meharg AA. 2009. Selenium in higher plants: understanding mechanisms for biofortification and phytoremediation. *Trends in Plant Science* 14(8):436−42
20. Xiao T, Qiang J, Sun H, Luo F, Li X, et al. 2024. Overexpression of wheat selenium-binding protein gene *TaSBP*-a enhances plant growth and grain selenium accumulation under spraying sodium selenite. *International Journal of Molecular Sciences* 25(13):7007
21. Lee JM, Kubota C, Tsao SJ, Bie Z, Echevarria PH, et al. 2010. Current status of vegetable grafting: diffusion, grafting techniques, automation. *Scientia Horticulturae* 127(2):93−105
22. Zhang T, Wang Y, Ma X, Ouyang Z, Deng L, et al. 2022. Melatonin alleviates copper toxicity via improving ROS metabolism and antioxidant defense response in tomato seedlings. *Antioxidants* 11(4):758
23. Zhang T, Sun K, Chang X, Ouyang Z, Meng G, et al. 2022. Comparative physiological and transcriptomic analyses of two contrasting pepper genotypes under salt stress reveal complex salt tolerance mechanisms in seedlings. *International Journal of Molecular Sciences* 23(17):9701
24. Li X, Luo Y, Zeng C, Zhong Q, Xiao Z, et al. 2023. Selenium accumulation in plant foods and selenium intake of residents in a moderately selenium-enriched area of Mingyueshan, Yichun, China. *Journal of Food Composition and Analysis* 116:105089
25. Kim D, Langmead B, Salzberg SL. 2015. HISAT: a fast spliced aligner with low memory requirements. *Nature Methods* 12(4):357−60
26. Sun H, Wu S, Zhang G, Jiao C, Guo S, et al. 2017. Karyotype stability and unbiased fractionation in the paleo-allotetraploid *Cucurbita* genomes. *Molecular Plant* 10(10):1293−306
27. Pertea M, Pertea GM, Antonescu CM, Chang TC, Mendell JT, et al. 2015. StringTie enables improved reconstruction of a transcriptome from RNA-seq reads. *Nature Biotechnology* 33(3):290−95
28. Love MI, Huber W, Anders S. 2014. Moderated estimation of fold change and dispersion for RNA-seq data with DESeq2. *Genome Biology* 15(12):550
29. Abbas HMK, Huang HX, Wang AJ, Wu TQ, Xue SD, et al. 2020. Metabolic and transcriptomic analysis of two *Cucurbita moschata* germplasms throughout fruit development. *BMC Genomics* 21(1):365
30. Jiang H, Lin W, Jiao H, Liu J, Chan L, et al. 2021. Uptake, transport, and metabolism of selenium and its protective effects against toxic metals in plants: a review. *Metallomics* 13(7):mfab040
31. Byeon Y, Lee HY, Lee K, Back K. 2014. Caffeic acid O-methyltransferase is involved in the synthesis of melatonin by methylating N-acetylserotonin in *Arabidopsis*. *Journal of Pineal Research* 57(2):219−27
32. Hawrylak-Nowak B, Matraszek R, Pogorzelec M. 2015. The dual effects of two inorganic selenium forms on the growth, selected physiological parameters and macronutrients accumulation in cucumber plants. *Acta Physiologiae Plantarum* 37(2):41
33. Van Hoewyk D, Takahashi H, Inoue E, Hess A, Tamaoki M, et al. 2008. Transcriptome analyses give insights into selenium-stress responses and selenium tolerance mechanisms in *Arabidopsis*. *Physiologia Plantarum* 132(2):236−53
34. Li HF, McGrath SP, Zhao FJ. 2008. Selenium uptake, translocation and speciation in wheat supplied with selenate or selenite. *New Phytologist* 178(1):92−102
35. Carey AM, Scheckel KG, Lombi E, Newville M, Choi Y, et al. 2012. Grain accumulation of selenium species in rice (*Oryza sativa* L.). *Environmental Science & Technology* 46(10):5557−64
36. Zhang L, Hu B, Li W, Che R, Deng K, et al. 2014. *OsPT2*, a phosphate transporter, is involved in the active uptake of selenite in rice. *New Phytologist* 201(4):1183−91
37. Inostroza-Blancheteau C, Reyes-Díaz M, Alberdi M, Godoy K, Rojas-Lillo Y, et al. 2013. Influence of selenite on selenium uptake, differential antioxidant performance and gene expression of sulfate transporters in wheat genotypes. *Plant and Soil* 369(1):47−59
38. Cao D, Liu Y, Ma L, Jin X, Guo G, et al. 2018. Transcriptome analysis of differentially expressed genes involved in selenium accumulation in tea plant (*Camellia sinensis*). *PLoS One* 13(6):e0197506
39. Kataoka T, Hayashi N, Yamaya T, Takahashi H. 2004. Root-to-shoot transport of sulfate in *Arabidopsis*. Evidence for the role of SULTR3;5 as a component of low-affinity sulfate transport system in the root vasculature. *Plant Physiology* 136(4):4198−204
40. Ren H, Li X, Guo L, Wang L, Hao X, et al. 2022. Integrative transcriptome and proteome analysis reveals the absorption and metabolism of selenium in tea plants [*Camellia sinensis* (L.) O. Kuntze]. *Frontiers in Plant Science* 13:848349
41. Oshanova D, Kurmanbayeva A, Bekturova A, Soltabayeva A, Nurbekova Z, et al. 2021. Level of sulfite oxidase activity affects sulfur and carbon metabolism in *Arabidopsis*. *Frontiers in Plant Science* 12:690830
42. Ren H, Zhang Y, Zhong M, Hussian J, Tang Y, et al. 2023. Calcium signaling-mediated transcriptional reprogramming during abiotic stress response in plants. *Theoretical and Applied Genetics* 136(10):210
43. Kudla J, Becker D, Grill E, Hedrich R, Hippler M, et al. 2018. Advances and current challenges in calcium signaling. *New Phytologist* 218(2):414−31
44. Ravi B, Foyer CH, Pandey GK. 2023. The integration of reactive oxygen species (ROS) and calcium signalling in abiotic stress responses. *Plant, Cell & Environment* 46(7):1985−2006
45. Wang C, Luan S. 2024. Calcium homeostasis and signaling in plant immunity. *Current Opinion in Plant Biology* 77:102485
46. Dard A, Weiss A, Bariat L, Auverlot J, Fontaine V, et al. 2023. Glutathione-mediated thermomorphogenesis and heat stress responses in *Arabidopsis thaliana*. *Journal of Experimental Botany* 74(8):2707−25
47. Bachhawat AK, Yadav S. 2018. The glutathione cycle: glutathione metabolism beyond the γ-glutamyl cycle. *IUBMB Life* 70(7):585−92
48. Li Y, Liu Y, Zhang J. 2010. Advances in the research on the AsA-GSH cycle in horticultural crops. *Frontiers of Agriculture in China* 4(1):84−90
49. Kumar S, Trivedi PK. 2018. Glutathione S-transferases: role in combating abiotic stresses including arsenic detoxification in plants. *Frontiers in Plant Science* 9:751
50. He X, Wang C, Wang H, Li L, Wang C. 2020. The function of MAPK cascades in response to various stresses in horticultural plants. *Frontiers in Plant Science* 11:952
51. Zhang M, Zhang S. 2022. Mitogen-activated protein kinase cascades in plant signaling. *Journal of Integrative Plant Biology* 64(2):301−41
52. Liu Y, Zhang S. 2004. Phosphorylation of 1-aminocyclopropane-1-carboxylic acid synthase by MPK6, a stress-responsive mitogen-activated protein kinase, induces ethylene biosynthesis in *Arabidopsis*. *The Plant Cell* 16(12):3386−99
53. Li G, Meng X, Wang R, Mao G, Han L, et al. 2012. Dual-level regulation of ACC synthase activity by MPK3/MPK6 cascade and its downstream *WRKY* transcription factor during ethylene induction in *Arabidopsis*. *PLoS Genetics* 8(6):e1002767
54. Takahashi F, Yoshida R, Ichimura K, Mizoguchi T, Seo S, et al. 2007. The mitogen-activated protein kinase cascade MKK3–MPK6 is an important part of the jasmonate signal transduction pathway in *Arabidopsis*. *The Plant Cell* 19(3):805−18
55. Jagodzik P, Tajdel-Zielinska M, Ciesla A, Marczak M, Ludwikow A. 2018. Mitogen-activated protein kinase cascades in plant hormone signaling. *Frontiers in Plant Science* 9:1387
56. Indumathi MC, Swetha K, Abhilasha KV, Siddappa S, Kumar SM, et al. 2024. Selenium ameliorates acetaminophen-induced oxidative stress via MAPK and Nrf2 pathways in mice. *Biological Trace Element Research* 202(6):2598−615
57. Colombage R, Singh MB, Bhalla PL. 2023. Melatonin and abiotic stress tolerance in crop plants. *International Journal of Molecular Sciences* 24(8):7447
58. Li MQ, Hasan MK, Li CX, Ahammed GJ, Xia XJ, et al. 2016. Melatonin mediates selenium-induced tolerance to cadmium stress in tomato plants. *Journal of Pineal Research* 61(3):291−302